Journal of The Electrochemical Society, **158** (10) H1090-H1096 (2011)
0013-4651/2011/158(10)/H1090/7/$28.00 © The Electrochemical Society

Self-Affine Surface Roughness of Chemically and Thermally Cleaned Ge(100) Surfaces

C. Fleischmann,[a,z] M. Houssa,[b,*] S. Sioncke,[c,] B. Beckhoff,[d] M. Müller,[d] P. Hönicke,[d] M. Meuris,[c] K. Temst,[a] and A. Vantomme[a]**

[a]*Instituut voor Kern- en Stralingsfysica and INPAC and* [b]*Semiconductor Physics Laboratory, K.U. Leuven, BE-3001 Leuven, Belgium*
[c]*IMEC, BE-3001 Leuven, Belgium*
[d]*Physikalisch-Technische Bundesanstalt, D-10587 Berlin, Germany*

An approach is presented to apply fractal concepts (by analyzing scanning length-dependent scanning tunneling microscopy measurements) to the characterization of semiconductor surfaces exposed to various, technologically relevant, cleaning processes. In particular, we have investigated the surface morphology and chemical composition of Ge(100) surfaces after cleaning in an aqueous HF solution and vacuum annealing. The roughness exponent α, a characteristic parameter to describe self-affine fractal surfaces, depends on the cleaning procedure and correlates to the surface chemical composition. For temperatures close to 500°C, atomic diffusion and desorption processes reduce the roughness exponent, which is equivalent to an increase in the sub-micron scale roughness. At temperatures above 500°C, surface smoothening mechanisms are initiated, leading to increasing roughness exponent values. In strong contrast, no pronounced changes in the surface roughness were observed on a large scale (saturation roughness), i.e. beyond the regime of self-affine scaling. Our findings highlight the significance of using scanning length-dependent roughness analysis to quantitatively assess variations in surface morphology after different cleaning processes and to directly compare various complex surfaces.
 [DOI: 10.1149/1.3624762]

Manuscript submitted July 21, 2011; revised manuscript received July 22, 2011. Published August 10, 2011.

Cleaning of semiconductor surfaces is of great importance from both scientific and technological perspective. In fact, surface cleaning is arguably the most frequently repeated process step during the fabrication of any semiconductor device. Besides the effective surface conditioning (removal of contaminants and surface termination), a quantitative assessment of the surface morphology upon various cleaning steps is likewise of particular concern. The surface roughness is a crucial parameter that can deteriorate surface/interface properties, and hence the device performance and reliability, as it may degrade charge carrier mobility or induce local high electric fields which lead to premature breakdown.[1] Needless to say that good knowledge about the physical and chemical processes that govern a cleaning step and their respective impact on the surface characteristics is of crucial importance.

A problematic issue in the measurement of the surface roughness is the lack of a uniform and consistent procedure, which allows comparison of various complex surfaces. Commonly used (amplitude) roughness parameters are e.g. the arithmetical mean height, root-mean square (rms) roughness or the peak-to-peak height of the surface.[2] However, the arrangement of atoms on a surface that results in a particular surface roughness parameter is not unique.[3] Moreover, these roughness parameters depend on the length scale of observation, i.e. for the same surface profile the roughness parameter may significantly change with the sampling length. For a proper evaluation of cleaning processes and their influence on the surface roughness, and hence on device performance, one should account for this fact since surfaces may appear smooth on a micrometer lateral length scale while rather coarse on a nanometer length scale, or vice-versa. It is, however, important to note that physical processes responsible for performance loss, e.g. charge-carrier scattering, tunneling or diffusion processes, take place precisely on this nanometer scale. Moreover, device dimensions such as the gate oxide thickness or the gate length, approach the nanometer regime nowadays,[4] implying that information of the surface properties on this length scale is likewise of paramount importance.

To characterize surfaces in a more comparable and objective way, and to account for the above described concerns, fractal theory proves very valuable. In fact, a wide variety of surfaces exhibit a roughness described by *self-affine fractal scaling*, i.e. the surfaces are invariant under anisotropic scale transformations.[3,5] Examples include the surfaces of vacuum deposited thin-films,[6–8] ion-bombarded films[9] or surfaces after wet-chemical etching.[10,11] For a self-affine surface the rms roughness σ increases with the lateral sampling length L according to the power law $\sigma \propto L^{\alpha}$, with α $(0 < \alpha < 1)$ being referred to as the *roughness exponent*.[3,5] This exponent is correlated to the texture of the surface on a sub-micron scale and quantifies how the roughness varies with scan length. A small α value is usually (within solid-state physics phenomena) indicative of a rough, jagged surface, whereas a large α is associated with locally smooth surfaces.[12] Moreover, self-affine surfaces exhibit a *lateral correlation length* ξ, above which σ may reach saturation (σ_{sat}) and does no longer scale with the sampling length L. Using this concept, even complex surfaces can be described and compared to a large extent using just one parameter, i.e. the roughness exponent α.

Up to now, various experimental techniques have been utilized for fractal analysis of surfaces, for an overview we refer to Ref. 3. Scanning probe microscopy techniques (SPM) are, however, the most appropriate methods as they can provide three-dimensional topographic data with high spatial resolution, allowing to evaluate the surface roughness on varying lateral length scales, typically ranging from the micrometer range down to the atomic scale. Moreover, these techniques can be applied on a wide variety of materials and in various environments (vacuum, air or liquid), that may be relevant in semiconductor technology. To determine the scaling exponent α, SPM images can be analyzed applying Fourier analysis, variational approaches, height difference correlation functions or by a direct measurement of the rms roughness versus scan size.[3] A variation on the latter approach is to subdivide the recorded SPM image into squares of decreasing dimensions and to extract the rms roughness from each of them. This method, in principle, enables the evaluation of scaling properties from a single SPM image.[13]

In this paper, we show that the concept of fractal analysis can be applied to evaluate cleaning processes and their impact on the characteristics of Ge surfaces. Germanium has recently received special attention as it is a promising candidate for the replacement of silicon channels in future high-performance microelectronic devices. Yet, detailed studies about the impact of standard cleaning methods on the morphology and composition of this surface remain scant. We

* Electrochemical Society Fellow.
** Electrochemical Society Active Member.
z E-mail: claudia.fleischmann@fys.kuleuven.be

have investigated the surface morphology and chemical composition of Ge(100) surfaces after performing wet-chemical cleaning in an aqueous HF solution and subsequent ultra-high-vacuum (UHV) annealing. In particular, scanning tunneling microscopy (STM) was applied to determine the scaling properties by a direct measurement of the surface roughness versus length scale $\sigma(L)$. This approach was complemented by Auger electron spectroscopy, allowing to identify atomic processes such as adsorption, surface reconstruction, diffusion or desorption that occur during these cleaning steps.

Methods

Experimental setup.—We used p-type (gallium) doped Ge(100) $\pm$ 0.5° substrates, which were immersed in 2% HF for 5 min without stirring, followed by a 1 min water rinse and a nitrogen blow dry. After wet-chemical cleaning we immediately loaded the samples into the respective analysis chamber for chemical or structural surface characterization. Sample annealing was performed in a vacuum chamber at temperatures between 200 and 800°C, applying a heating rate of 5°C/min, while maintaining the chamber pressure below 1E-7 Torr. The temperature was read out with a thermocouple at the backside of the molybdenum sample holder. The annealing chamber is equipped with a mass spectrometer allowing to perform temperature programmed desorption (TPD) measurements to detect desorption products as a function of annealing temperature.

To verify whether hydrogen-termination was achieved upon HF cleaning we used multiple internal reflection Fourier transform infrared spectroscopy (MIR FT-IR). The MIR geometry allows to significantly enhance the surface sensitivity as the IR beam is reflected several times on the surface. We used a double-sided, polished Ge(100) wafer cut to 1 mm $\times$ 26 mm $\times$ 92 mm with both edges beveled to 45°, which results in about 100 internal reflections. FT-IR spectra were recorded over a wavenumber ranging between 500 and 4000 cm^{-1} with a resolution of 1 cm^{-1}, using a nitrogen cooled mercury cadmium telluride (HgCdTe) detector. All spectra were referenced to an untreated Ge wafer with approximately 2–3 nm native oxide layer. The chamber pressure during measurements was kept constant around 2 Torr.

Identification of residual surface impurities after chemical and physical cleaning steps was achieved with Auger electron spectroscopy (AES) using an Alpha 110 hemispherical analyser from Thermo Scientific. In the same vacuum chamber a reverse view low-energy electron diffraction (LEED) system is installed, allowing to investigate the specific surface reconstruction after each treatment.

Information on the depth distribution of impurities, such as oxygen and carbon, was obtained using grazing incidence x-ray fluorescence (GIXRF). These measurements were carried out in the PTB laboratory at the synchrotron radiation facility BESSY II in Berlin (Germany) at the plane grating monochromator beamline (PGM-U49) for undulator radiation. For detailed information on the experimental conditions and setup we refer to Refs. 14–16. We recorded the angular dependence of the O K_α and C K_α fluorescence radiation with the incident photon energy set to 1060 eV and the angle of incidence varying between 0° and 4.2°.

The surface morphology and scaling behavior were investigated using a large sample (LS) UHV STM from Omicron. STM images were recorded at room temperature in constant-current mode using a PtIr tip with a sample bias voltage around 3.5 V and a tunneling current around 0.3 nA. Image processing was done using the Scanning Probe Image Processor (SPIP) (roughness analysis) and WSXM (Ref. 17) (visualization) software. To investigate scaling properties, the following procedure was used: After each surface preparation step multiple STM images ranging from 50 to 1000 nm in scan length were recorded at random locations on the surface. All images were plane fitted to account for macroscopic slopes present in the images and the rms roughness was evaluated. Subsequently, all images were divided into squares of decreasing linear dimension L and the rms surface roughness $\sigma(L)$ was computed for each of them. Images that showed atypical large defects, contamination or other irregularities have been removed from the data set. The average σ over all images with the same dimension is finally plotted against L in a double-logarithmic plot from which α and σ_{sat} were determined.

Sample annealing and subsequent AES, STM and LEED measurements were performed in the same UHV system with a base pressure of 1E-10 Torr. Only the MIR FT-IR and the GIXRF measurements were performed in separate systems.

Theoretical calculations.—The OH/Ge(100) interface model was generated from first-principles molecular dynamics (MD) simulations, as implemented in the Siesta simulation package,[18] using density functional theory within the local density approximation for the exchange-correlation functional[19] and a Nosé thermostat, with a 1 fs time step. The core electrons were implicitly treated by using norm-conserving pseudopotentials,[20] and the valence electrons were described by using double-zeta singly polarized (DZP) basis sets, considering the following electronic configuration of the elements: H $1s^1$, O $(1s^2)$ $2s^2$ $2p^4$, and Ge (Ar $3d^{10}$) $4s^2$ $4p^2$, where the core configurations are shown in parenthesis. A plane wave cutoff of 250 Ry and a $(4 \times 4 \times 1)$ k-point mesh were used for the computations, assuring convergence of the total energy of the system below typically 10 meV. We started from a (2×1) reconstructed Ge(100) surface, modeled using slabs of 6 Ge layers, with the bottom slab passivated by hydrogen atoms, and about 15 Å of vacuum above the surface (2×2 supercell, corresponding to 64 atoms). The surface was then gradually loaded with oxygen atoms, and the MD simulations were performed at 300 K, during typically a few ps. The remaining Ge dangling bonds are saturated by hydrogen atoms. *Mercury* 2.3 was used to visualize the atomistic models obtained by the MD simulations.[21]

Results and Discussion

Chemical cleaning.—Chemical composition.—Prior to characterization of the scaling behavior we investigated the chemical composition of the surface after wet-chemical cleaning. From AES measurements (Fig. 1) we deduced that the Ge(100) surface after immersing in hydrofluoric acid contains traces of carbon (272 eV) and oxygen (510 eV). Residual surface oxides after wet-chemical treatment are often reported in literature and we will discuss this issue in more detail below. Carbon is similarly reported to be one of the most common impurities on Ge(100) surfaces, with the initial

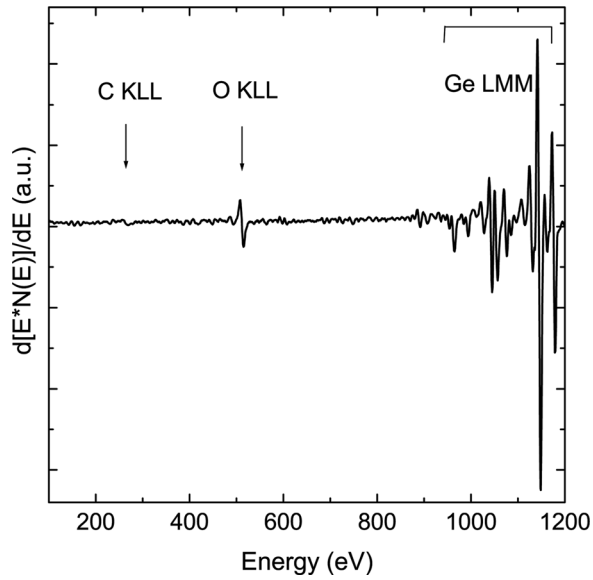

Figure 1. Auger electron spectrum measured on a Ge(100) surface after cleaning in diluted HF solution.

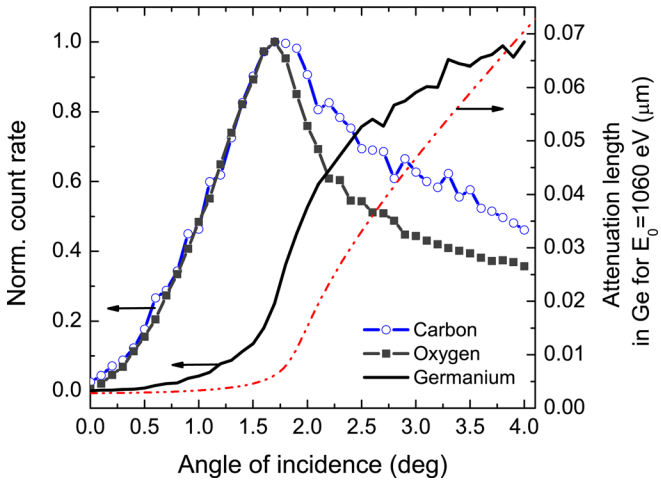

Figure 2. (Color online) GIXRF angular scan on a Ge(100) surface after cleaning in diluted HF solution showing the evolution of the C K_α fluorescence line (open circles), the O K_α fluorescence line (closed squares) and the Ge L fluorescence line (solid line) with angle of incidence. The dash-dotted line shows the attenuation length of x-rays with an incoming energy E_0 = 1060 eV in a Ge crystal.

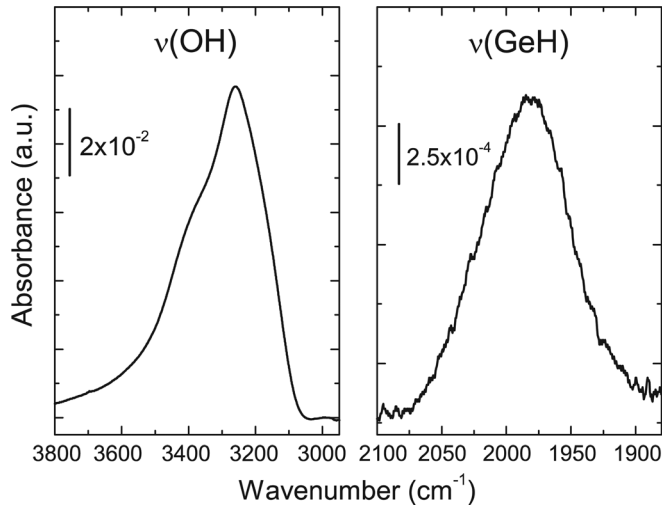

Figure 3. MIR FT-IR spectra recorded on a Ge(100) surface after cleaning in diluted HF solution showing the ν(OH) (left) as well as the ν(GeH) vibration mode (right).

carbon concentration being strongly affected by the preparation conditions (solution quality, air purification, etc.).[22–28] A GIXRF angular scan (Fig. 2) confirms that oxygen is solely accumulated on the surface. The carbon signal, on the other hand, emerges from deeper in the substrate, as can be seen from the slower decline of the count rate with increasing angles. This may indicate that this signal does not merely originate from adventitious carbon adsorbed on the surface during wet-chemical preparation, but also from C impurities within the bulk. Even though the solubility of C in Ge is rather low (10^8–10^{10} cm^{-3}), it has been reported that carbon can be introduced in the Ge lattice during crystal growth.[4] This observation suggests that not only surface impurities but also bulk impurities need to be accounted for, in particular during annealing studies.

The removal of native or chemically grown GeO_2 using HF solution has been studied for more than a decade. Whereas GeO_2 can be easily dissolved in water,[29] acidic[30] or alkaline solution,[31] the removal of sub-oxides is much more challenging. Most of the studies[28,32–34] agree that hydrofluoric acid does neither remove all sub-oxides, nor produce stable H-termination as has been reported for silicon. In contrast, the Ge surface is best described by an inhomogeneous hydrogen layer co-existing with an oxide layer. This model is also confirmed by our own experiments. MIR FT-IR measurements (Fig. 3) reveal a positive absorbance peak centered around 1984 cm^{-1}, which can be assigned to the ν(GeH) vibration mode and implies adsorption of hydrogen on the Ge surface upon HF treatment.[35] The ν(GeH) band can be fitted by a single, broad Gaussian peak, which indicates a predominant formation of a single GeH_x phase on the surface, i.e. mono-hydride [1987 cm^{-1}, (Ref. 27)]. It has been reported in literature that the formation of di-hydrides [2020 cm^{-1}, (Ref. 27)] on the Ge(100) surface is only stable if the surface exhibits a high defect density or surface roughness, as is the case for example for sputtered surfaces[36] or surfaces etched with highly concentrated (>10%) HF solutions.[37] On flat surfaces, steric repulsion between the H atoms of adjacent GeH_2 species would significantly reduce the stability of this phase.[36] A similar effect might be expected for adjacent GeO areas, which could likewise lower the stability of di-hydrides on the surface. The broad, intense peak around 3260 cm^{-1} is associated with the ν(OH) vibration band. This is an indication for water adsorption or hydroxyl-termination and hence a rather hydrophilic surface. As termination with hydrides is expected to yield a hydrophobic surface, this can be a sign of incomplete hydrogen termination and residual surface oxides after HF cleaning. The ν(GeO) vibration band is located around 750–1050 cm^{-1}. Our measurements show a negative absorbance band in this wavelength range after H_2O or HF dipping (data not shown). A negative absorbance is equivalent to a reduction in the oxygen content (GeO) compared to an untreated Ge wafer (reference spectrum), even though this yields no quantitative information about the oxide removal. However, from previous x-ray absorption spectroscopy measurements we know that the HF treated surfaces are not free of GeO.[14] In fact, after this cleaning step the Ge surface contains traces of hydrogen, oxygen and carbon (organic contaminants) and exhibits a hydrophilic rather than a hydrophobic character.

Atomic structure.—It can be intuitively expected that the co-existence of the above described surface species (i.e. H and O) may impact the atomic structure on the HF cleaned Ge surface. In an attempt to investigate the atomic arrangement on these complex surfaces in more detail, we have performed MD simulations. In these simulations we only accounted for the presence of oxygen and hydrogen atoms, whereas carbon impurities were disregarded. The reason for this is the difficulty to precisely assign the oxidation state of carbon on the surface, and hence its local bonding configuration. In general, an adsorbate-free Ge(100) surface exhibits a (2 × 1) surface reconstruction as the top-most atoms rearrange within the surface plane, thereby forming Ge dimers.[38] An atomistic model of such a dimerized Ge(100) surface is depicted in Figs. 4a and 4b.

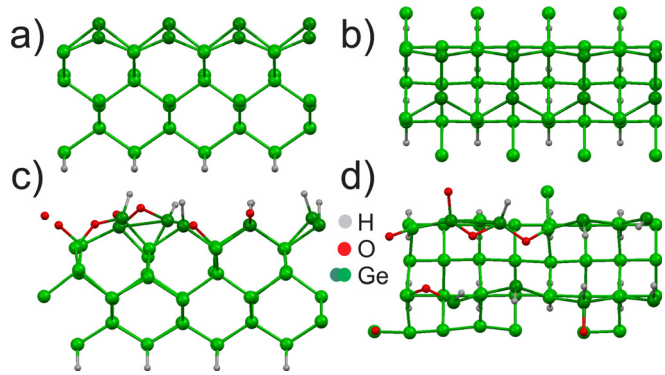

Figure 4. (Color online) Atomic geometries as obtained from molecular dynamics simulations and/or structural relaxations shown in side- (left) and top-view (right). (a) and (b) clean Ge(100)-(2 × 1) surface. (c) and (d) OH/Ge(100) surface.

Upon adsorption of heteroatoms this (2×1) dimer reconstruction can be lifted, depending on the specific adsorption conditions and coverage. This is illustrated in Figs. 4c and 4d, in which the atomic configuration of the Ge(100) surface after partial oxygen and hydrogen adsorption is shown. It can be instantly inferred from this figure that the atomic order on this OH/Ge surface changes drastically compared to the adsorbate-free surface (Figs. 4a and 4b). In particular, it is observed that the Ge dimer bonds are broken after (i) the chemisorption of oxygen and hydrogen atoms and (ii) the formation of Ge-O-Ge bridging bonds on the surface. As these Ge-H and Ge-O bonds do not show any preferential orientation on the surface, probably due to steric hindrance, long-range atomic order is impeded. This OH/Ge model, generated by MD simulations, should be representative of a real Ge(100) surface after an HF treatment (see discussion above). STM measurements on the HF cleaned Ge surface, shown in Fig. 5a, likewise confirm the absence of long-range atomic order. Hence, our results imply that treatment in HF solution does not yield complete hydrogen-terminated, i.e. hydrophobic surfaces with high atomic order, due to the co-existence of residual Ge-O bonds and the random orientation of these chemical bonds on the surface. These findings are in strong contrast to hydrogenation performed under UHV conditions, where the Ge dimer bonds and atomic order are preserved after exposure to atomic hydrogen at room temperature.[36]

Surface roughness.—Besides revealing the surface atomic arrangement, STM was also used to investigate the surface roughness on a micrometer to nanometer scale. The evolution of the rms roughness σ with scan length L of the HF cleaned Ge surface is shown in a double-logarithmic plot in Fig. 6 (open squares). σ increases with increasing sampling length L, followed by saturation beyond the cross-over point ξ. From this behavior we conclude that the Ge(100) surface after cleaning in diluted HF solution follows self-affine scaling, with $\alpha = (0.44 \pm 0.07)$ and $\sigma_{sat} = (0.32 \pm 0.01)$ nm.

Theoretical models that describe self-affine surface roughening by wet-chemical etching processes and predict respective roughness exponents are rather scarce. An example is the study by Santra and Sapoval, in which it was shown that the interface between a finite-etching solution and a random solid presents a fractal morphology at the end of the etching process.[39] Cafiero et al. presented a model for chemical etching of crystalline silicon including an anisotropy parameter to account for the intrinsic anisotropy of etching rates.[40] This model predicts roughness exponents ranging from 0.63 (for isotropic systems) to 0.93 (for completely anisotropic systems), which

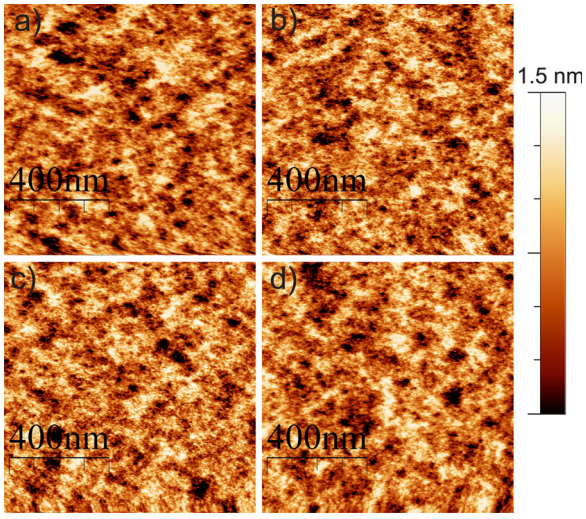

Figure 5. (Color online) STM measurements on a Ge(100) surface (a) after wet-chemical etching in diluted HF solution as well as after subsequent vacuum annealing at (b) 500°C (c) 700°C and (d) 800°C. All images were recorded at room temperature.

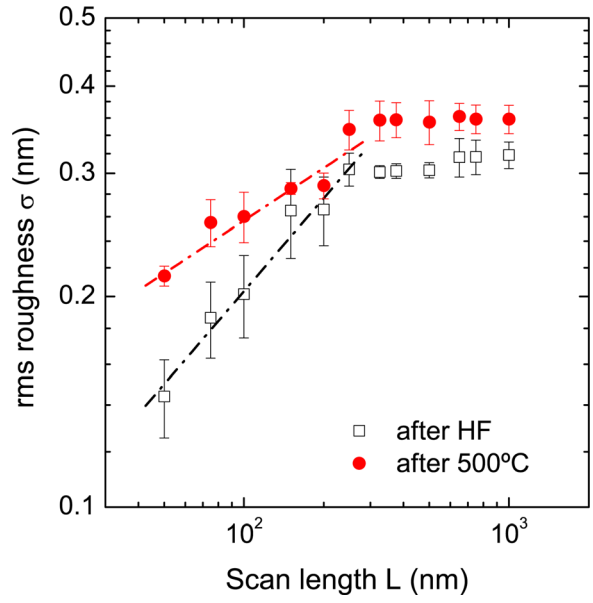

Figure 6. (Color online) Evolution of rms surface roughness σ with scan length L after cleaning in diluted HF solution (open squares) and after subsequent vacuum annealing to 500°C (filled circles).

are however not in agreement with our experimental result. The model proposed by Kessler et al. describes a fluid interface propagating through a random medium.[41] Depending on the effective propagation velocity, α reaches values between 0.5 (for high velocities) and 0.76 (for low velocities). This model was used successfully by Dotto and Kleinke to describe surface morphology evolution in silicon etching processes.[11] In our study, samples have been immersed in solution without stirring or forced convection using an ultrasonic bath. Hence, the propagation velocity of the etch process is expected to be rather low. According to the model proposed by Kessler et al. this should yield a roughness exponent close to 0.76, which disagrees with our experimental finding. The discrepancy between the experimental value and the roughness exponents predicted by theory may be caused by differences between the experimental conditions and the conditions assumed by these models. Yet, the determination of a roughness exponent after each surface treatment, i.e. chemical or physical cleaning, allows for a qualitative and quantitative comparison of various complex surfaces and to discern relative variations in the surface morphology. For a better comparison of the experimental values with theory, theoretical models may need to be further developed to account for the respective experimental conditions.

Thermal cleaning.—Chemical composition and surface roughness.—After the wet-chemical cleaning in HF solution, we subsequently annealed the sample in small temperature steps up to 800°C. The surface roughness $\sigma(L)$ was evaluated after each annealing step. In general, the surface exhibits a self-affine topography after each temperature step, hence the evolution of σ with scan length L is comparable to what is found after the wet-chemical treatment. An example of $\sigma(L)$ of the surface after annealing to 500°C is shown in Fig. 6 (closed circles). It can be inferred from this figure that there is no change in the overall scaling behavior. There are, however, minor variations in the initial slope, i.e. α. An overview of the α values extracted from the STM measurements after each annealing step is shown in Fig. 7 (stars). As the roughness exponent describes the surface topography on sub-micron scale, we assign the variation in α upon annealing to temperature-induced, local atomic re-arrangements on the surface. In particular, α reaches a minimum value at 500°C, which can be associated with a maximum in the sub-micron scale roughness. Hence, the surface is more jagged compared to the initial state after wet-chemical cleaning. Further

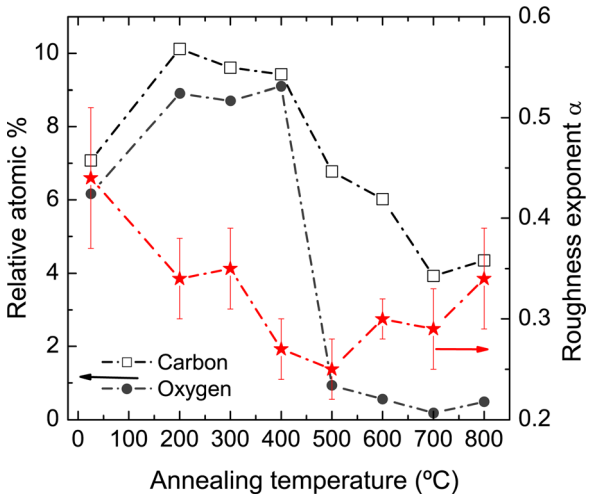

Figure 7. (Color online) Evolution of the roughness exponent α with annealing temperature (right axis) in comparison to the O KLL and C KLL AES signal (left axis).

annealing increases the roughness exponent, i.e. smoothens the surface again.

Upon annealing, surface diffusion, decomposition of surface phases or desorption processes can occur, which may influence the local atomic arrangement and hence smoothen or roughen the surface. A correlation between the roughness exponent and the chemical surface composition, i.e. the oxygen and carbon AES signal intensity, is evident from Fig. 7 (closed circles, open squares). It is apparent from this graph that the minimum value for α coincides with a significant drop in the oxygen and carbon AES signal. The removal of physisorbed species, such as water or carbon/oxygen-containing surface species adsorbed during the wet-chemical treatment, can be easily achieved by a mild annealing (< 300°C) and may be the origin of the initial decrease in α. In contrast, complete removal of oxygen chemically bonded to the Ge surface is reported to occur at temperatures above 400°C,[22,42–44] and proceeds through the desorption of GeO.[22,44,45] This is also confirmed by our TPD study shown in Fig. 8, in which GeO is detected as a desorption product upon annealing. The two distinct peaks in the TPD spectrum are an indication for two different kinetic processes that lead to GeO

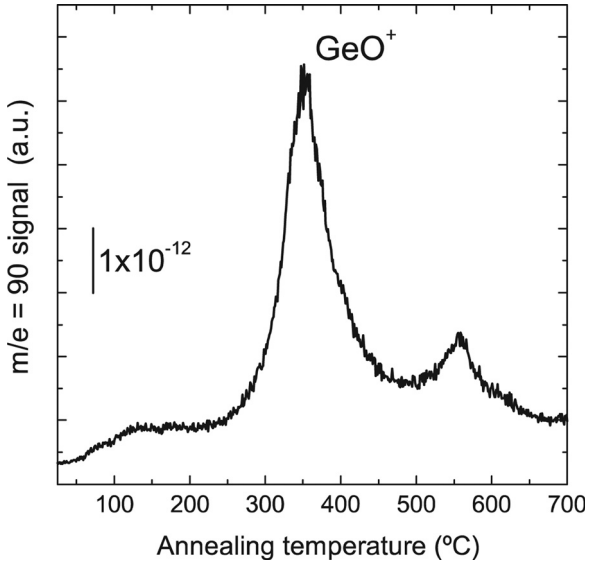

Figure 8. TPD spectrum of GeO (m/e = 90) collected from a Ge(100) surface after cleaning in diluted HF.

desorption.[43,45] It has been postulated by Hansen and Hudson that desorption of GeO primarily occurs from defect sites with the oxygen species diffusing towards these sites.[45] Hence, the desorption mechanism initiates atomic re-arrangement and local etching processes as Ge atoms leave the surface. This explains the reduction in α, or the increase in surface roughness on the atomic scale in this temperature range. At temperatures above 500°C, however, the mobility of Ge surface atoms is enhanced, leading to migration of surface atoms and temperature-dependent smoothening mechanisms.[46] This accounts for the decrease in surface roughness on the submicron scale and hence the increase in the roughness exponent.

Atomic structure.—The Ge(100)– (2 × 1) surface reconstruction is restored after oxygen desorption, as evident from the LEED diffraction pattern shown in Fig. 9a. However, STM measurements after annealing to 800°C (Figs. 9b, 9c) reveal that the surface still lacks long-range atomic ordering, nor can large, smooth terraces be observed. In addition, bright protrusions with an apparent height between 4 and 6 Å can be found in the STM image. Based on previous studies[23,26] and due to the fact that the surface is not free of carbon impurities (Fig. 7), we assign these protrusions to carbon clusters. These impurities may cause pinning of step movement during annealing, which hampers the formation of large terraces and a (2 × 1) dimer reconstruction on larger scale. In contrast to oxygen impurities, carbon is not easily desorbed upon annealing.[23] Besides, GIXRF measurements (Fig. 2) have indicated that carbon is not only accumulated on the surface but also present within the substrate. Annealing the substrate at elevated temperature can lead to enhanced carbon diffusivity and surface segregation of carbon atoms. This has been observed, e.g. by Wei et al., who studied carbon-implanted germanium substrates.[47] The authors report on the surface migration of carbon and a surface aggregation as nano-sized graphite clusters after annealing at 500°C. As the diffusivity and aggregation of carbon atoms increase upon annealing, these carbon clusters will grow in size at the expense of smaller clusters, therefore decreasing the surface roughness. This likewise coincides with the observation that α increases at temperatures above 500°C.

In summary, we have demonstrated that HF cleaned and vacuum annealed Ge(100) surfaces exhibit self-affine fractal behavior. Using this concept we were able to disentangle the complex atomic processes that impact the sub-micron scale surface morphology. In particular, it was shown that desorption of physisorbed and chemisorbed surface species (< 500°C) causes an increase in the surface roughness, whereas continuous annealing at higher temperatures initiates atomic diffusion and smoothening mechanisms. In strong contrast, beyond the regime of self-affine scaling no variations have been observed in the saturation roughness σ_{sat}. This is apparent from Fig. 10, which shows the temperature dependence of the rms roughness extracted from (1000 × 1000) nm^2 STM images. Large

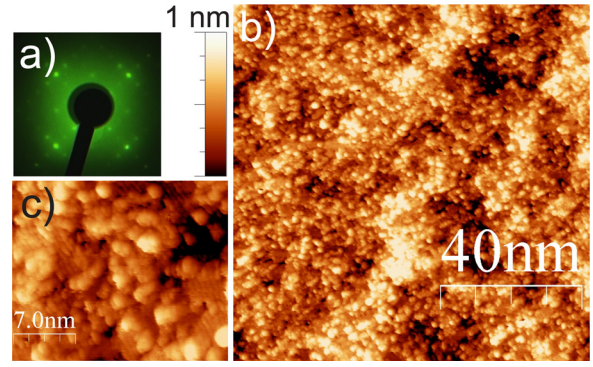

Figure 9. (Color online) (a) LEED diffraction pattern on a Ge(100) surface after cleaning in diluted HF solution and subsequent vacuum annealing to 500°C. (b) STM measurements on the same surface as in (a) after vacuum annealing to 800°C. (c) An enlarged area of the image shown in (b).

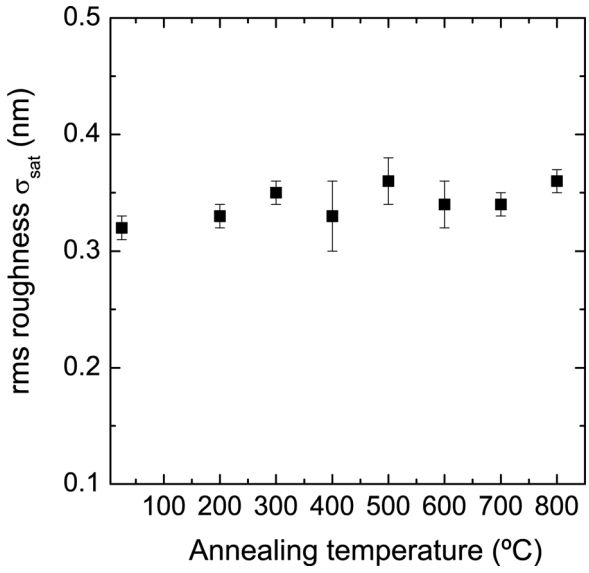

Figure 10. Saturation rms roughness σ_{sat} for different annealing temperatures.

scale STM measurements after various annealing steps do likewise reveal no significant changes in the surface morphology (Figs. 5b–5d).

Conclusions

We have presented a thorough investigation of the surface chemical composition and morphology of Ge(100) surfaces after wet-chemical cleaning and vacuum annealing steps. The co-existence of oxygen- and hydrogen terminated areas, present after cleaning in an aqueous HF solution, drastically impedes the long-range atomic ordering on the surface and results in a hydrophilic surface. The wet-chemical cleaning step leaves organic contaminants, which may form agglomerates on the surface upon thermal treatments. We have shown that Ge(100) surfaces exhibit a self-affine morphology after wet-chemical cleaning and subsequent vacuum annealing. The roughness exponent α was found to vary with the annealing temperature. We assigned these variations to temperature-induced surface diffusion and desorption processes of surface atoms. On a submicron scale, these processes cause an increase in surface roughness for annealing temperatures between 200 and 500°C. At higher temperature, surface diffusion and aggregation of surface atoms smoothen the surface. On a large scale, however, no significant variation in the surface morphology could be observed. These findings clearly demonstrate the power of measuring scanning length-dependent roughness parameters and the use of scaling theory to quantitatively investigate variations in surface morphology upon a cleaning process. For surface cleaning and conditioning this is of special importance, as chemically clean surfaces may exhibit defects and increased roughness at the atomic scale, which may, however, not be revealed at large scales. In the particular case of an initially wet-chemically cleaned Ge(100) surface, subsequent annealing to temperatures close to 500°C will be sufficient to remove surface oxides and to initiate a (2×1) atomic reconstruction, but not to prepare a smooth surface, required for further processing steps and proper device functioning.

We have shown that the approach of fractal analysis of SPM data allows for precise and reliable characterization of the surface morphology and a direct comparison of complex surfaces exposed to different cleaning processes. With this, we were able to disentangle the interplay between chemical and physical atomic processes in a cleaning sequence, and, additionally, to what extent these processes influence surface properties that determine device performance, e.g. roughness and composition. This procedure provides a platform for evaluating and optimizing cleaning methods and process parameters, such as temperature, in order to prevent yield and performance losses.

Acknowledgments

This work has been supported by the Research Foundation - Flanders (FWO, Belgium), by the Belgium Interuniversity Attraction Poles (IAP P6/42), the K.U.Leuven BOF (CREA/07/005) program as well as by the Flemish Concerted Action (GOA/09/006) research programs. C.F. has received additional support from the K.U. Leuven centre of excellence Institute for Nanoscale Physics and Chemistry (INPAC, Grant No. EF/05/005). The grazing incidence x-ray fluorescence measurements were supported by the European Commission-Research Infrastructure Action under the FP6 "European Integrated Activity of Excellence and Networking for Nano- and Micro-Electronics Analysis" - Project number 026134 (RI3) ANNA.

References

1. T. Low, M. Li, G. Samudra, C. Yeo, C. Zhu, A. Chin, and D. L. Kwong, *IEEE Trans. Electron Devices*, **52**, 2430 (2005).
2. G. Barbato, K. Carneiro, D. Cuppini, J. Garnaes, G. Gori, G. Hughes, C. P. Jensen, J. F. Jørgensen, O. Jusko, S. Livi, et al., *Scanning Tunneling Microscopy Methods for Roughness and Micro Hardness Measurements* (European Commission Catalogue number: CD-NA-16145 EN-C, Brussels Luxemburg, 1995).
3. J. Krim and G. Palasantzas, *Int. J. Mod. Phys. B*, **9**, 599 (1995).
4. C. Claeys and E. Simoen, *Germanium Based Technologies*, Elsevier, New York (2007).
5. A. L. Barabási and H. E. Stanley, *Fractal Concepts in Surface Growth*, Cambridge University, New York (1995).
6. K. Temst, M. J. Van Bael, B. Wuyts, C. Van Haesendonck, Y. Bruynseraede, D. G. de Groot, N. Koeman, and R. Griessen, *Appl. Phys. Lett.*, **67**, 3429 (1995).
7. A. Vantomme, J. E. Mahan, G. Langouche, J. Becker, M. Van Bael, K. Temst, and C. Van Haesendonck, *Appl. Phys. Lett.*, **70**, 1086 (1997).
8. S. M. Jordan, R. Schad, D. J. L. Herrmann, J. F. Lawler, and H. van Kempen, *Phys. Rev. B*, **58**, 13132 (1998).
9. J. Krim, I. Heyvaert, C. Van Haesendonck, and Y. Bruynseraede, *Phys. Rev. Lett.*, **70**, 57 (1993).
10. L. Spanos and E. A. Irene, *J. Vac. Sci. Technol. A*, **12**, 2646 (1994).
11. M. E. R. Dotto and M. U. Kleinke, *Phys. Rev. B*, **65**, 245323 (2002).
12. J. Krim and J. O. Indekeu, *Phys. Rev. E*, **48**, 1576 (1993).
13. M. V. H. Rao, B. Mathur, and K. L. Chopra, *Appl. Phys. Lett.*, **64**, 124 (1994).
14. C. Fleischmann, S. Sioncke, S. Couet, K. Schouteden, B. Beckhoff, M. Müller, P. Hönicke, M. Kolbe, C. Van Haesendonck, M. Meuris, et al., *J. Electrochem. Soc.*, **158**, H589 (2011).
15. B. Beckhoff, *J. Anal. At. Spectrom.*, **23**, 845 (2008).
16. P. Hönicke, B. Beckhoff, M. Kolbe, D. Giubertoni, J. van den Berg, and G. Pepponi, *Anal. Bioanal. Chem.*, **396**, 2825 (2010).
17. I. Horcas, R. Fernández, J. M. Gómez-Rodríguez, J. Colchero, J. Gómez-Herrero, and A. M. Baro, *Rev. Sci. Instrum.*, **78**, 1 (2007).
18. J. M. Soler, E. Artacho, J. D. Gale, A. García, J. Junquera, P. Ordejón, and D. Sánchez-Portal, *J. Phys.: Condens. Matter*, **14**, 2745 (2002).
19. D. M. Ceperley and B. J. Alder, *Phys. Rev. Lett.*, **45**, 566 (1980).
20. N. Troullier and J. L. Martins, *Phys. Rev. B*, **43**, 1993 (1991).
21. C. F. Macrae, P. R. Edgington, P. McCabe, E. Pidcock, G. P. Shields, R. Taylor, M. Towler, and J. van de Streek, *J. Appl. Crystallogr.*, **39**, 453 (2006).
22. R. E. Schlier and H. E. Farnsworth, *J. Chem. Phys.*, **30**, 917 (1959).
23. S. Gan, L. Li, T. Nguyen, H. Qi, R. F. Hicks, and M. Yang, *Surf. Sci.*, **395**, 69 (1998).
24. T. Deegan and G. Hughes, *Appl. Surf. Sci.*, **123/124**, 66 (1998).
25. J. S. Hovis, R. J. Hamers, and C. M. Greenlief, *Surf. Sci.*, **440**, L815 (1999).
26. L. H. Chan, E. I. Altman, and Y. Ling, *J. Vac. Sci. Technol. A*, **19**, 976 (2001).
27. S. Rivillon, Y. J. Chabal, F. Amy, and A. Kahn, *Appl. Phys. Lett.*, **87**, 253101 (2005).
28. S. Sun, Y. Sun, Z. Liu, D. I. Lee, S. Peterson, and P. Pianetta, *Appl. Phys. Lett.*, **88**, 021903 (2006).
29. K. Prabhakaran and T. Ogino, *Surf. Sci.*, **325**, 263 (1995).
30. H. Okumura, T. Akane, and S. Matsumoto, *Appl. Surf. Sci.*, **125**, 125 (1998).
31. T. Akane, J. Tanaka, H. Okumura, and S. Matsumoto, *Appl. Surf. Sci.*, **108**, 303 (1997).
32. K. Choi and J. M. Buriak, **16**, 7737 (2000).
33. D. Bodlaki, H. Yamamoto, D. H. Waldeck, and E. Borguet, *Surf. Sci.*, **543**, 63 (2003).
34. B. Onsia, T. Conard, S. De Gendt, M. Heyns, I. Hoflijk, P. Mertens, M. Meuris, G. Raskin, S. Sioncke, I. Teerlinck, et al., *Solid State Phenom.*, **103–104**, 27 (2005).
35. Y. J. Chabal, *Surf. Sci.*, **168**, 594 (1986).
36. J. Y. Maeng, J. Y. Lee, Y. E. Cho, and S. Kim, *Appl. Phys. Lett.*, **81**, 3555 (2002).
37. K. Park, Y. Lee, and S. Lim, *Applied Surface Science.*, **254**, 1842 (2008).
38. H. J. W. Zandvliet, *Phys. Rep.*, **388**, 1 (2003).
39. S. B. Santra and B. Sapoval, *Physica A*, **266**, 160 (1999).
40. R. Cafiero, V. Loreto, and P. P. Prosni, *Europhys. Lett.*, **42**, 389 (1998).

41. D. A. Kessler, H. Levine, and Y. Tu, *Phys. Rev. A*, **43**, 4551 (1991).
42. A. J. Rosenberg, P. H. Robinson, and H. C. Gatos, *J. Appl. Phys.*, **29**, 771 (1958).
43. K. Prabhakaran, F. Maeda, Y. Watanabe, and T. Ogino, *Appl. Phys. Lett.*, **76**, 1 (2000).
44. K. Kita, C. H. Lee, T. Nishimura, K. Nagashio, and A. Toriumi, *ECS Trans.*, **19**(2), 101 (2009).
45. D. A. Hansen and J. B. Hudson, *Surf. Sci.*, **292**, 17 (1993).
46. K. M. Horn, E. Chason, J. Y. Tsao, S. T. Floro, and J. A. Picraux, *Surf. Sci.*, **320**, 174 (1994).
47. P. Wei, Y. Xu, S. Nagata, K. Narumi, and H. Naramoto, *Nucl. Instrum. Methods Phys. Res. B*, **206**, 233 (2003).